Variable-node axisymmetric solid element and its application to adaptive mesh refinement

Chang-Koon Choi† and Eun-Jin Lee‡

Department of Civil Engineering, KAIST, Taejon 305-600, Korea

Wan-Hoon Lee‡†

Department of Civil & Environment Engineering, Chungwoon University, Chungnam 350-701, Korea

Abstract. This paper presents an effective application of a variable-node axisymmetric solid element designated as AQV (Axisymmetric Quadrilateral Variable-node element). The variable-node element with physical midside nodes helps to overcome some problems in connecting the different layer patterns on a quadrilateral mesh in the adaptive *h*-refinement. This element alleviates the necessity of imposing displacement constraints on irregular (hanging) nodes in order to enforce the inter-element compatibility. Therefore, the elements with variable mid-side nodes can be used effectively in the local mesh refinement for the axisymmetric structures which have stress concentrations. A modified Gaussian quadrature should be adopted to evaluate the stiffness matrices of the variable-node elements mainly because of the slope discontinuity of assumed displacement within the elements. Some numerical examples show the usefulness of variable-node axisymmetric elements in the practical application.

Key words: quadrilateral axisymmetric element; irregular node; variable-node element; transition element; adaptive *h*-refinement.

1. Introduction

The axisymmetric elements have been used in various fields of engineering. In aerospace engineering, the elements have been applied to perform the stress analysis of solid propellant grains, rocket nozzles and cases, spacecraft bulkheads and heat shields, etc. In mechanical engineering, they have been applied to thick-walled pipes, storage tanks, pressure vessels, pistons, rotors, etc. In civil engineering, they have been applied to tunnels, thick-walled pipes in soil, half-space, cylindrical and spherical types of structures, etc. And there are many other problems in the different engineering fields for which the asiymmetric element can be effectively used.

In such various engineering practices, stress concentration phenomena occur at the areas where there are abrupt geometrical changes, or at the points under concentrated loading. In order to solve this type of problem, a relatively finer grid is used in the areas of high stress gradients, while a rather rough grid is used where the stress distribution is relatively uniform. There are several

---

† Institude Chair Professor
‡ Graduate Student
‡† Professor

possible ways to generate a locally refined finite element grid by using quadrilateral elements.

A rectangular shaped element was used to generate locally refined mesh in a way that the two layers of subdivided rectangular elements are connected to an undivided larger element (Bathe 1982, Hughes 1987). In this case, one corner node of subdivided elements that can not be connected to the side of the larger element which does not have a physical node at the midside may have to be generated. These nodes are termed irregular (or hanging) nodes. To preserve the compatibility between the refined and unrefined meshes in this case, linear dependencies between the unknown nodal displacements should be introduced by applying constraints to the force-displacement equation (Choi and Kim 1992, Choi and Lee 1993).

Zienkiewicz *et al*. (1991) used the meshing techniques which use some distorted isoparametric elements in the transition zone without any constraints. However, it should be noted that the performance of isoparametric element is generally at its best when used without the shape distortion. Although the effect of distorted elements on the accuracy of the solution depends to a large degree on the types of problems considered and the elements used, it is desirable to refine the mesh locally without producing distorted elements.

Using the mixed mesh which consists of different element types for local mesh refinement, for example, a mixed use of quadrilateral elements and triangular elements in the transition zone, could be another possibility for mesh gradation as practiced by many investigators (Yunus *et al*. 1990, Evans *et al*. 1991). The triangular elements, however, may show worse results than the quadrilaterals in general, and the introduction of triangular elements to the mesh that consist mostly of quadrilateral elements can degrade the solution even if the quadrilaterals work well.

Choi and Park (1989, 1992) effectively used the quadrilateral variable-node plate elements which have a variable number of additional nodes on the edges of a basic 4-node plate bending element to connect directly to different layer patterns. Their concepts of variable-node plate elements are extended to be used in the axisymmetric problems.

In this study, the use of variable-node axisymmetric solid element, which is designated as AQV (Axisymmetric Quadrilateral Variable-node element) in the formulation of transition zone is presented. Algorithms for the stress smoothing and adaptive mesh refinement techniques using AQV-element are also proposed in the adjusted form of the existing techniques. The merits of the devised variable-node axisymmetric element in this study can be viewed from the several numerical examples with a transition zone.

2. Element formulation

2.1 Axisymmetric quadrilateral element

An axisymmetric solid is defined as a three-dimensional body that is developed by rotation of a planar section about an axis. Cylindrical coordinates r, z, and θ provide a suitable reference frame definition for the axisymmetric solids. The body is assumed to be axisymmetric with respect to the z axis and that the typical finite element is a form of circular ring. This element may have various cross-sectional shapes, and if the loads are axisymmetric, the ring is analyzed using a representative two-dimensional section only.

Translational displacements u and w occur in the r and z directions, respectively, while the transformation in the θ direction is zero. In addition, the shearing strains $\gamma_{r\theta}$ and $\gamma_{z\theta}$ are zeros as
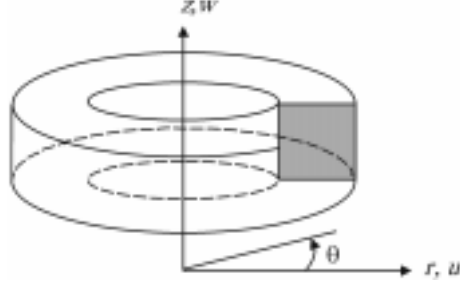
Fig. 1 An axisymmetric quadrilateral element

well. For An axisymmetric quadrilateral element as shown in Fig. 1, the displacement functions are assumed to be the same as the two-dimensional isoparametric element. The displacement field $\boldsymbol{u}$ can be expressed by shape function matrix $[N]$ and nodal displacement vector $\{d\}$ as follows:

$$\boldsymbol{u}=\begin{Bmatrix} u \\ w \end{Bmatrix}=\begin{Bmatrix} \Sigma N_i u_i \\ \Sigma N_i w_i \end{Bmatrix}=[N]\{d\} \tag{1}$$

where the definitions of N_i are found in Eq. (11). The nonzero strains are as follows:

$$\boldsymbol{\varepsilon}=\langle \varepsilon_r, \varepsilon_z, \varepsilon_\theta, \gamma_{rz} \rangle^T$$

Relationships between these strains and the displacements are:

$$\varepsilon_r=\frac{\partial u}{\partial r}, \quad \varepsilon_z=\frac{\partial w}{\partial z}$$

$$\varepsilon_\theta=\frac{2\pi(r+u)-2\pi r}{2\pi r}=\frac{u}{r}, \quad \gamma_{rz}=\frac{\partial u}{\partial z}+\frac{\partial w}{\partial r} \tag{3}$$

and the strain matrix is given in the form of

$$\boldsymbol{\varepsilon}=[B]\{d\} \tag{4}$$

where,

$$[B_i]=\begin{bmatrix} \dfrac{\partial N_i}{\partial r} & 0 \\ 0 & \dfrac{\partial N_i}{\partial z} \\ \dfrac{N_i}{r} & 0 \\ \dfrac{\partial N_i}{\partial z} & \dfrac{\partial N_i}{\partial r} \end{bmatrix} \tag{5}$$

The corresponding stresses to the strains in Eq. (2) are:

$$\boldsymbol{\sigma}=\langle \sigma_r, \sigma_z, \sigma_\theta, \tau_{rz} \rangle^T \tag{6}$$

and the stress-strain relationship may be expressed in a matrix form as

$$\boldsymbol{\sigma} = [D]\boldsymbol{\varepsilon} \tag{7}$$

where for an isotropic material, the matrix $[D]$ is simplified to

$$[D] = \frac{E}{(1+\mu)(1-\mu)} \begin{bmatrix} 1-\mu & \mu & \mu & 0 \\ \mu & 1-\mu & \mu & 0 \\ \mu & \mu & 1-\mu & 0 \\ 0 & 0 & 0 & 1/2-\mu \end{bmatrix}$$

The stiffness matrix is finally obtained as

$$[K] = \int_A \int_0^{2\pi} [B][D][B] |J| r \, d\theta \, dA \tag{9}$$

where $|J|$ is the determinant of Jacobian.

2.2 Variable-node element

The local mesh refinement using the quadrilaterals is performed with a relative ease by bisecting a mother element into four child elements as shown in Fig. 2 (Choi and Lee 1996). Then some corner nodes of the new-born elements have irregular (or hanging) nodes, marked as crosses in Fig. 2, which are not connected to the physical node of mother element. When the linear 4-node elements are used, the displacement constraint equation as given in Eq. (10) is imposed on the node c in Fig. 2 to preserve interelement compatibility along the side a-c-b.

$$\{u\}_c = \frac{1}{2}(\{u\}_a + \{u\}_b) \tag{10}$$

This approach was successfully used for the adaptive h-refinement in the past. However, this approach needs some modification of element stiffness matrix and load vector due to the introduction of constraint equations, and results in additional computations (Abel and Shephard 1979). In addition, the bandwidth of global stiffness matrix will be enlarged and too many constraints may lock the system (Cook 1981).
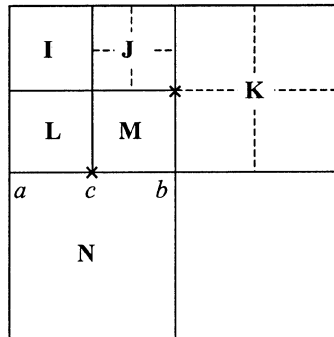

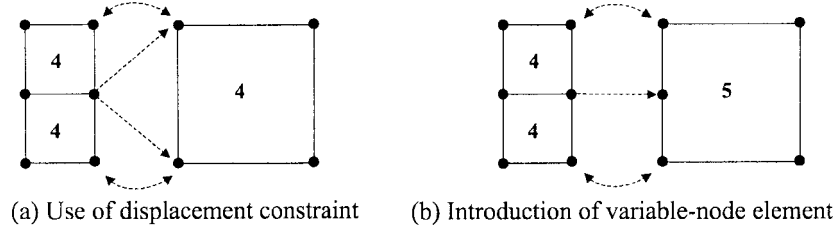Fig. 2 Local mesh refinement in quadrilateral mesh

(a) Use of displacement constraint   (b) Introduction of variable-node element

Fig. 3 Connection of different mesh layer

o midside node
● corner node

4-node element   5-node element   6-node element   7-node element
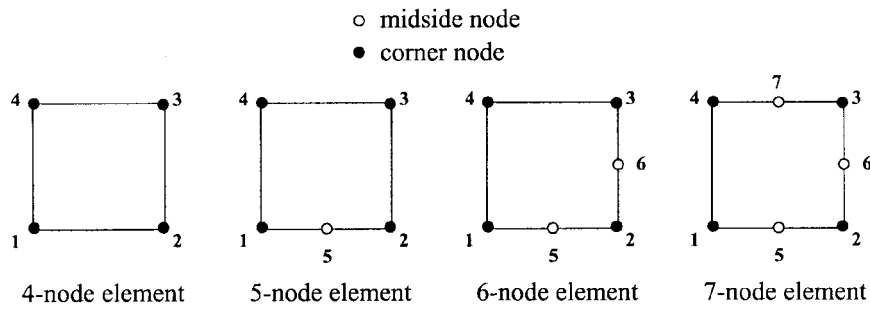
Fig. 4 The variable-node elements

If the unrefined 4-node element which is neighbored by the subdivided elements (Fig. 3a) is replaced by the variable-node element which has a midside node (Fig. 3b), additional computation as well as modification of existing finite element routines due to imposing the compatibility can be kept to the minimum (Choi and Park 1992, Choi and Lee 1995). And the locking due to the constraint equations can be avoided. The numbers inside the element in Fig. 3 indicate the number of nodes per element.

The possible variable-node quadrilateral axisymmetric elements are shown in Fig. 4. When a coarse mesh is connected to a refined mesh (Fig. 3), the discontinuous displacement field is defined over the variable-node axisymmetric elements so that the compatibility along the interelement boundary can be preserved. The shape functions for the variable-node axisymmetric elements are written as

$$\hat{N}_i = \frac{1}{4}(1 + \xi_i \xi)(1 + \eta_i \eta), \tag{11a}$$

$$\hat{N}_k = \frac{1}{2}(1 + |\xi_k| \xi_k \xi - |\eta_k| |\xi|)(1 + |\eta_k| \eta_k \eta - |\xi_k| |\eta|), \tag{11b}$$

$$N_i = \hat{N}_i - \frac{1}{2}(\hat{N}_j + \hat{N}_k), \tag{11c}$$

$$N_k = \hat{N}_k, \tag{11d}$$

where, $i=1, 2, 3, 4$, $j=\text{aint}(1/i) \times 4 + i + 3$, $k=i+4$ (11e)

In Eq. (11), $\hat{N}$ is the basic shape function and N is the final shape function which is actually used in the element matrix formulation. If the mid-side node does not exist on any element edge, the corresponding shape function should become zero (For 5-node elements; $N_6 = N_7 = 0$). With these shape functions, the basic variable-node axisymmetric solid element can be formulated. The element
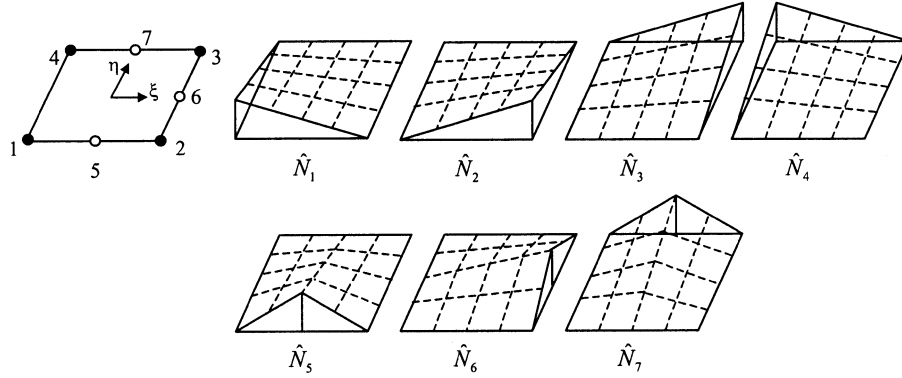
Fig. 5 The shape functions of the variable-node elements

is designated as AQV-element (Axisymmetric Quadrilateral Variable-node element) in this study.

2.3 Numerical integration

In evaluating the stiffness matrix of variable node axisymmetric element, a normal (usual) numerical integration may not be applied directly over the entire element domain ($-1 \leq \xi$, $\eta \leq +1$) because the slope discontinuity of displacement assumed in the element may cause a singular integral. Therefore, the Gaussian quadrature needs to be modified to be carried out over each sub-domain first and assembled later to form the entire element stiffness matrix. The coordinates and corresponding weight coefficients for the modified Gaussian quadrature points are given in Table 1 (Gupta 1978). For a single domain (the case of 4-node element), a 2×2 Gaussian quadrature is used. A one point integration rule or reduced integration, whose single Gauss point is located at the element center, makes the element display a mechanism and therefore should be avoided. The 5-node element can be divided into two sub-domains, while the 6-node or the 7-node element is divided into four sub-domains as shown in Fig. 6(b), 6(c) and 6(d) with dashed lines as boundaries of sub-domains. For the sake of simple programming, however, a 4×4 modified Gaussian quadrature may be used for the 5-node element as well as the 6-node and the 7-node element.

The load vector for the variable-node elements should also be evaluated in accordance with the aforementioned modified Gaussian quadrature.
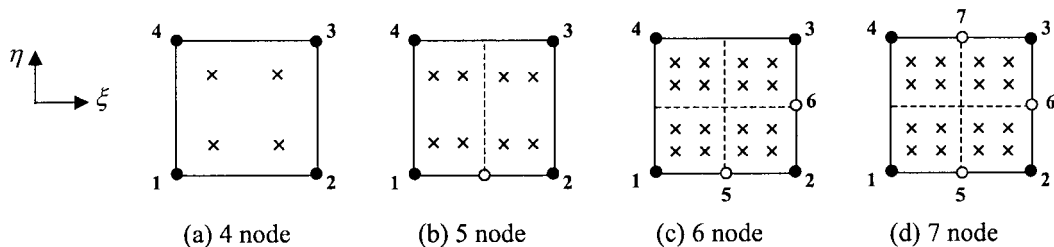

(a) 4 node　　　　(b) 5 node　　　　(c) 6 node　　　　(d) 7 node

Fig. 6 Gauss Point for variable-node elements

Table 1 Modified Gaussian quadrature for variable-node elements

ξ_i, η_l	Weight		ξ_i, η_l	Weight
−0.5773503 +0.5773503	1.0 for each point	$\rightarrow$ Modified	−0.7886761 −0.2113249 +0.2113249 +0.7886761	0.5 for each point
(a) For single domain			(b) For sub-domain	

3. Adaptive *h*-refinement using AQV-element

3.1 Adaptive mesh refinement

To improve the finite element solution, *h*-refinement strategy is frequently used in many practical problems where the order of element is kept constant and the mesh is locally refined to reduce element size *h*. When an error indicator for an element is larger than the user-specified upper error criterion, the element is refined. The refinement indicator ξ_i for element *i* is defined as Eq. (12)

$$\xi_i = \frac{\eta_i}{\bar{\eta}} = \frac{\|e_\sigma\|_i}{\left[\left(\sqrt{\|u\|^2 + \|e_\sigma\|^2}\right)/nel\right]^{1/2} \bar{\eta}} \tag{12}$$

where η_i is the relative error in percents for each element defined in Eq. (19) and $\bar{\eta}$ is the permissible relative error in percents. The value of $\bar{\eta}$ is generally somewhere between 5% and 10% in many engineering problems (Zienkiewicz and Zhu 1989). When the refinement indicator ξ_i exceed 1.0, the element should be refined to be suited for the permissible relative error.

The single-level difference rule (SLDR) is commonly used in the *h*-refinement to preserve the gradual variation of element sizes. The basic concept of SLDR can be briefly explained as shown in Fig. 7. When the element A need to be refined (Fig. 7a), in order to avoid violation of the SLDR, the element B should be refined prior to the refinement of element A (Fig. 7b).

3.2 Error estimation and stress smoothing

The stress error, on which the refinement indicator is based, is derived from the simple error estimation (Zienkiewicz and Zhu 1987), which is defined by the difference between the continuous smoothed stress σ^* and the finite element stress σ_h for an element since the exact stress field is
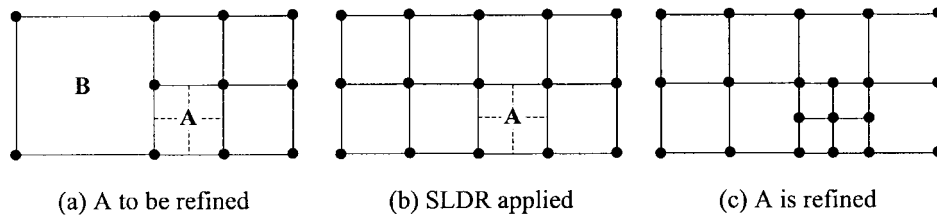

(a) A to be refined   (b) SLDR applied   (c) A is refined

Fig. 7 Single-level difference rule

generally not known.

$$e_\sigma = (\sigma^* - \sigma_h) \tag{13}$$

where the continuous stress field σ^* is defined by the same shape functions used for displacement field assumption in Eq. (11) and the smoothed nodal stresses σ_i^* are determined by Eq. (25).

$$\sigma^* = \sum N_i \sigma_i^* \tag{14}$$

The stress error of an element is defined by the energy norm of strain energy as

$$\|e_\sigma\|_i = \left(\int_{\Omega_i} (e_\sigma)^T D^{-1} (e_\sigma) d\Omega \right)^{1/2} = \left(\int_{\Omega_i} (\sigma^* - \sigma_h)^T D^{-1} (\sigma^* - \sigma_h) d\Omega \right)^{1/2} \tag{15}$$

and the error of entire solution domain $\|e_\sigma\|$ is calculated by summing up the error of each element.

$$\|e_\sigma\| = \left(\sum_{i=1}^{nel} \|e_\sigma\|_i^2 \right)^{1/2} \tag{16}$$

where *nel* is the total number of elements.

The relative percentage error of solution is estimated using the error norm and the strain energy norm of entire solution domain.

$$\eta = \frac{\|e_\sigma\|}{\sqrt{\|u\|^2 + \|e_\sigma\|^2}} \times 100(\%) \tag{17}$$

where,

$$\|u\| = \left(\sum_{i=1}^{nel} \|u\|_i^2 \right)^{1/2} = \left(\int_{\Omega_i} \sigma^T D^{-1} \sigma \, d\Omega \right)^{1/2} \tag{18}$$

The local error indicator for *i*-th element η_i is defined in a similar way

$$\eta_i = \left(\frac{\|e_\sigma\|_i^2}{\left(\sqrt{\|u\|^2 + \|e_\sigma\|^2} \right)/nel} \right)^{1/2} \times 100(\%) \tag{19}$$

If any element whose error indicator is larger than the predetermined permissible value, it should be refined. The systematic refinement for a quadrilateral element can be easily achieved by bisecting in two directions.

In this study, the superconvergent patch recovery procedure (Zienkiewicz and Zhu 1992) is specially modified to obtain σ^* for transition zone which is composed of variable-node elements. Fig. 8(a) shows a patch composed of Gauss points of the elements surrounding the patch assembly node, and Fig. 8(b) shows the patch composed of elements which have different level of refinement. The nodal value of continuous stress field σ^* is assumed to belong to a polynomial expansion σ_p^* of the complete order p which is valid in the patch. This polynomial expansion is used for each component of σ_p^*.

$$\sigma_p^* = Pa \tag{20}$$

where P contains the appropriate polynomial terms according to the complete p and a is a set of unknown parameters.

$$P = [1, r, z, rz] \qquad : (p=1)$$

$$P = [1, r, z, r^2, rz, z^2, r^2z, rz^2, r^2z^2] \qquad : (p=2) \tag{21}$$

$$a = [a_1, a_2, a_3, \ldots, a_{np-1}]^T \tag{22}$$

The unknown parameters a of the expansion given in Eq. (20) is best determined by ensuring a least square fit of this to the set of superconvergent sampling points. Through the procedure of least square fit, the unknown parameters a can be solved in a matrix form as

$$a = A^{-1}b \tag{23}$$

where,

$$A = \sum_{i=1}^{npts} P^T(r_i, z_i) P(r_i, z_i), \quad b = \sum_{i=1}^{npts} P(r_i, z_i) \sigma_h(r_i, z_i) \tag{24}$$

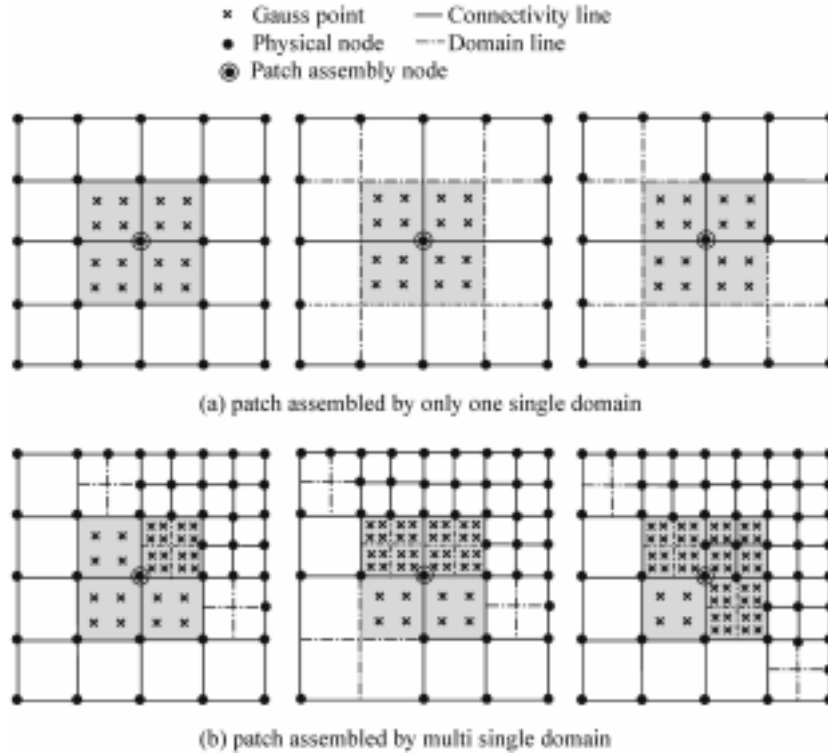where $npts$ is the number of total Gauss points of the patch. The continuous smoothed nodal

(a) patch assembled by only one single domain

(b) patch assembled by multi single domain

Fig. 8 Patch composed by Gauss points of AVQ-elements

stresses σ_i^* of the *i*-th node in the patch are given by

$$\sigma_i^* = P(r_i, z_i)a \tag{25}$$

Substituting σ_i^* into Eq. (14), the continuous smoothed stress can be obtained.

If the target node is placed on the boundary, the similar procedure is performed in some changes of *npts*.

4. Numerical tests for AQV-element

4.1 Eigenvalue test

The eigenvalue test is carried to check if the stiffness matrices of variable-node elements have correct ranks. The eigenvalue test can detect the zero-energy deformation modes, lack of invariance, and absence of rigid-body motion capability of the tested element. Through the eigenproblem for element stiffness, the eignevlaues which represent the rigid-body motion should be zero. For axisymmetric elements, the translation in z-direction is the only possible rigid body motion because of axial symmetry and accordingly, only one eigenvalue should be zero. Elements developed in this study, i.e., the AQV-elements, are shown to have only one zero eigenvalue and have no extra zero-energy mode.

4.2 Patch test

The patch test is a simple test that can be performed numerically so as to check the validity of element formulation and its programming implementation. A thick-walled cylinder with an arbitrary mesh is shown in Fig. 9. The boundary displacement is given to be $u=2r$ and $w=1+4z$, which may lead to zero shear stress. The test results, as listed in Table 2, show that the present element passes the patch test. The different positions of variable nodes (Figs. 9b, 9c and 9d) did not affect the results at all. Hence, the AQV-element passed the patch test.
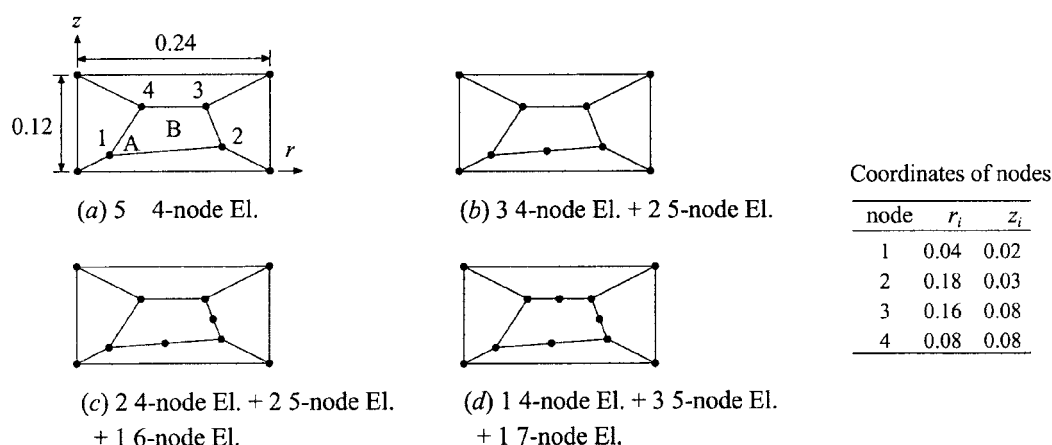

(*a*) 5 4-node El.   (*b*) 3 4-node El. + 2 5-node El.

Coordinates of nodes		
node	r_i	z_i
1	0.04	0.02
2	0.18	0.03
3	0.16	0.08
4	0.08	0.08

(*c*) 2 4-node El. + 2 5-node El.   (*d*) 1 4-node El. + 3 5-node El.
   + 1 6-node El.   + 1 7-node El.

Fig. 9 Patch test model (*E*=1000; *v*=0.25)

Table 2 Results of the patch test

Model	Displacement at point A		Stresses at point B			
	U_A	V_A	σ_{rB}	σ_{zB}	$\sigma_{\theta B}$	τ_{rzB}
(a)	0.08000	1.08000	480.000	640.000	480.000	0.000
(b)	0.08000	1.08000	480.000	640.000	480.000	0.000
(c)	0.08000	1.08000	480.000	640.000	480.000	0.000
(d)	0.08000	1.08000	480.000	640.000	480.000	0.000
Exact	0.08000	1.08000	480.000	640.000	480.000	0.000

4.3 MacNeal-Harder test

The MacNeal-Harder test (MacNeal and Harder 1985) is frequently used to check the effect of nearly incompressible material. An infinitely long thick-walled cylinder under the internal pressure is analyzed by taking a slice of unit thickness. Fig. 10(a) and 10(b) show the regular mesh and the irregular mesh, respectively and Fig. 10(c) shows the meshes with different positions of variable nodes.

Table 3 shows the normalized results (radial displacement at point A) of the analysis using the AQV-elements. All the present elements for both regular and irregular meshes are not free from the
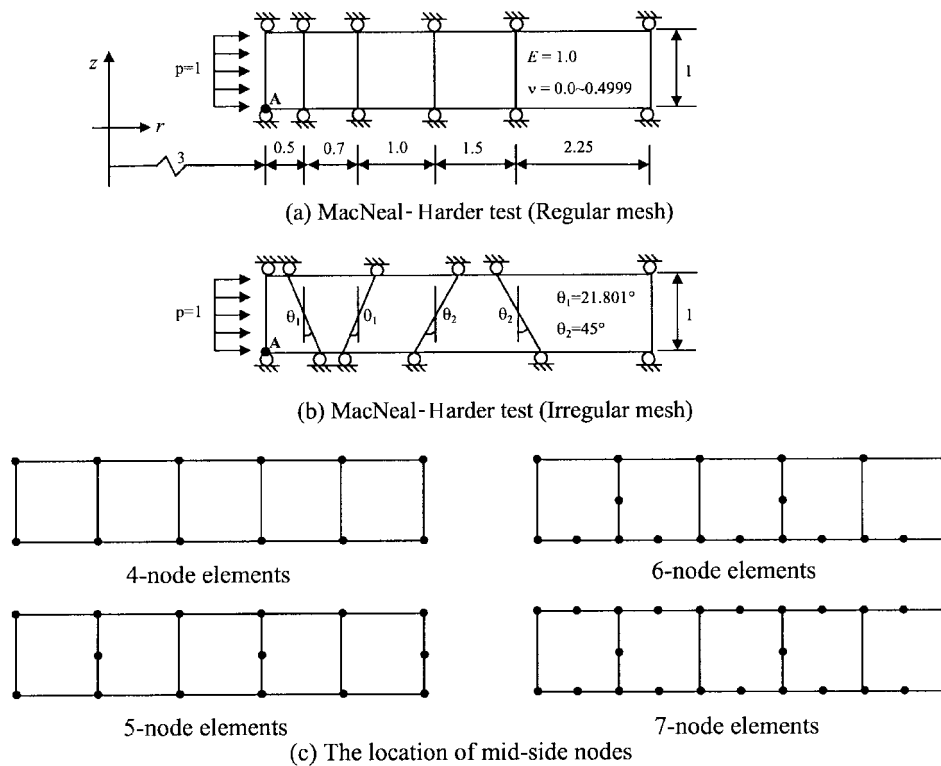

(a) MacNeal-Harder test (Regular mesh)

(b) MacNeal-Harder test (Irregular mesh)

(c) The location of mid-side nodes

Fig. 10 Thick-walled cylinder under internal pressure

Table 3 MacNeal-Harder test

n	(a) regular				(b) irregular mesh			
	4-node	5-node	6-node	7-node	4-node	5-node	6-node	7-node
0.0	0.994	0.994	0.999	0.998	0.990	0.989	1.004	1.009
0.3	0.988	0.988	0.991	0.991	0.982	0.980	0.988	0.995
0.49	0.847	0.846	0.856	0.870	0.817	0.833	0.823	0.857
0.499	0.361	0.360	0.387	0.428	0.317	0.365	0.340	0.411
0.4999	0.053	0.053	0.057	0.066	0.045	0.055	0.048	0.064

locking for the incompressible materials. This may indicate that the standard displacement formulation of elastic problems fails when Poisson's ratio v approaches 0.5 or when the material becomes incompressible. A simple way of side-stepping the difficulty associated with the material incompressibility is to use values of v approximating to 0.5 but not equal to it. The AQV-elements show reasonable accuracy until $v = 0.49$.

4.4 Test for bending action

An evenly loaded circular plate with simply supported edge is used to examine the bending actions. The plate is modeled by two different mesh divisions as given in Fig. 11 (Wanji and Cheung 1996). The meshes of variable nodes in Fig. 10(c) are also used.

Table 4 shows each of the computed transverse displacements at point A (Fig. 11a and 11b). Under the bending action, the variable-node element AQV shows a false shear phenomenon, but some
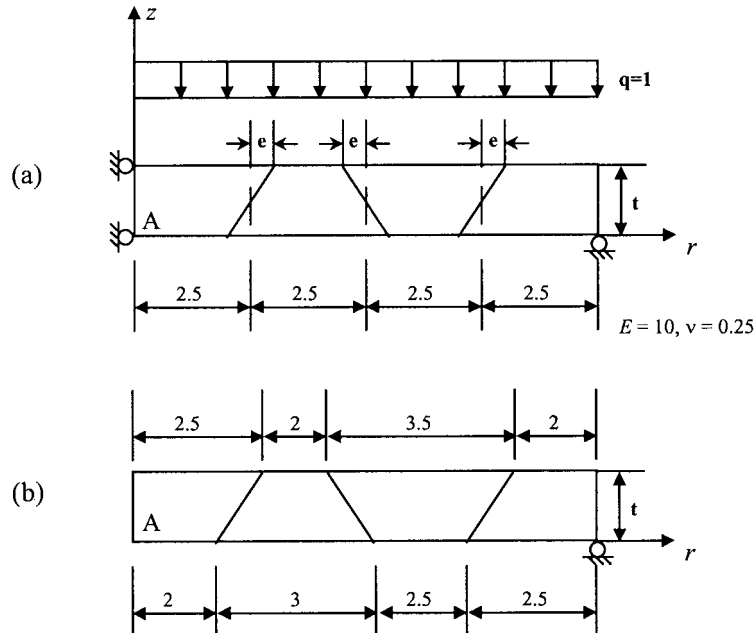

Fig. 11 Simply supported uniformly loaded circular plate

Table 4 Result for uniform loaded circular plate (Fig. 11a and 11b, $t=1$)

Element		w_A		
		(a) $e=0$	(a) $e=0.025$	(b)
AQV	4-node	−506.44	−505.38	−461.12
	5-node	−543.53	−542.25	−489.13
	6-node	−570.04	−570.25	−548.08
	7-node	−644.93	−644.58	−621.70
Exact			−738.28	

improvement in results is shown as to increase of the number of midside nodes. All the AQV-elements are much sensitive to element distortions.

5. Application for practical engineering problems

5.1 Pressure vessel

A pressure vessel is a kind of structure, which is most frequently modeled by axisymmetric elements in the engineering practice. Nuclear reactors, storage tanks and boiler structures are handled as a pressure vessel. In this study, a relatively simple prototype pressure vessel with uniform internal pressure is considered.

Due to the symmetry, only one-quarter of the vessel is actually analyzed. The section shape, boundary conditions and load conditions are given in Fig. 12. And the adaptive *h*-refinement process with a permissible relative error $\bar{\eta}$ of 7% at each element is carried out. The gradually refined meshes using AQV-elements are shown in Fig. 13(a) along with the deformed shapes and stress contours in Fig. 13(b) and 13(c). In these figures, *NI* is the number of iterations for the adaptive routine, η is the relative percentage error of the whole solution domain, and *ND* is the total number of degrees of freedom of the whole solution domain. It can be seen that the initial uniform mesh is gradually refined near the corner where the dense effective stress contours are observed. As the *h*-refinement proceeds, the relative percentage error decreases and the effective stress contour
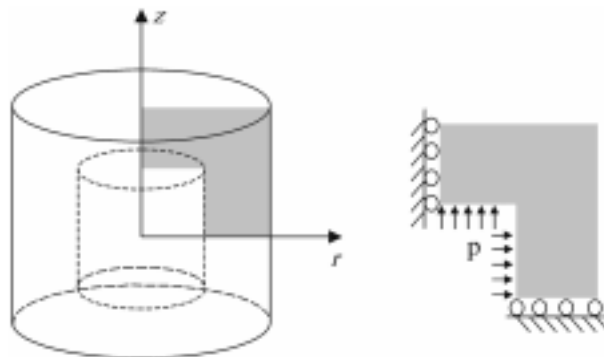

Fig. 12 A simple protoptype pressure vessel

(a) Locally refine mesh

(b) Deformed shape (×5000)
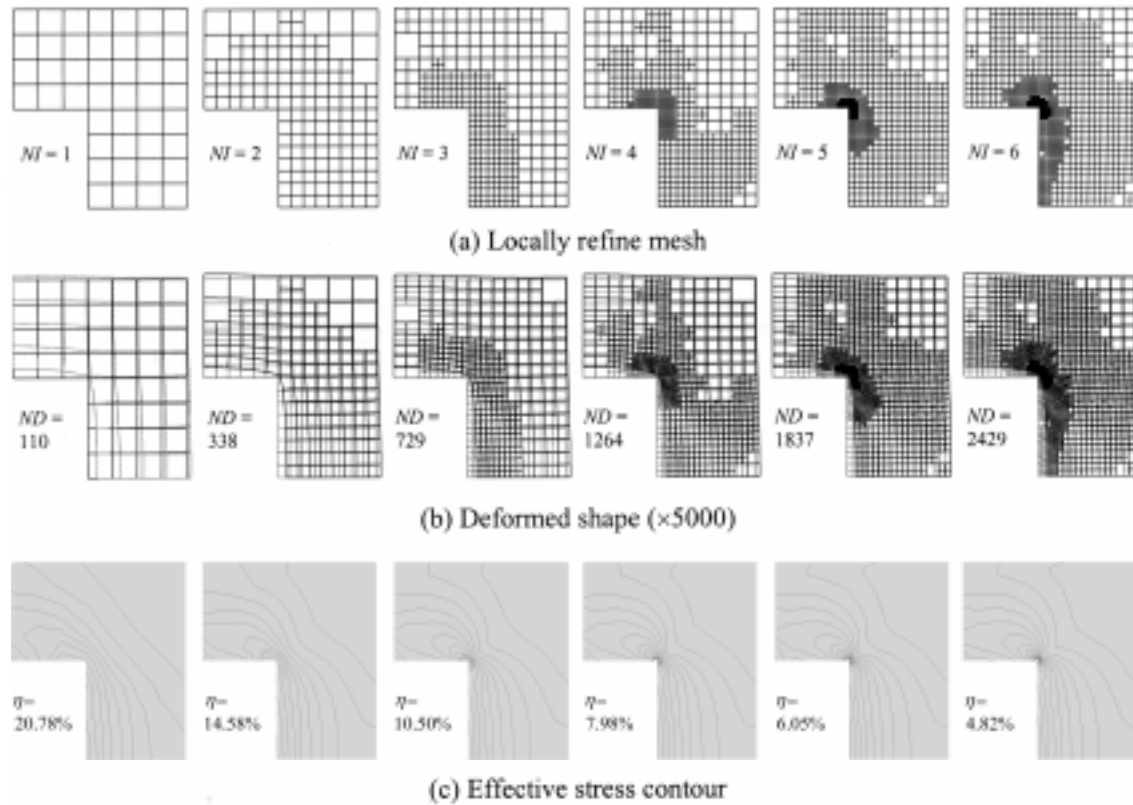

(c) Effective stress contour

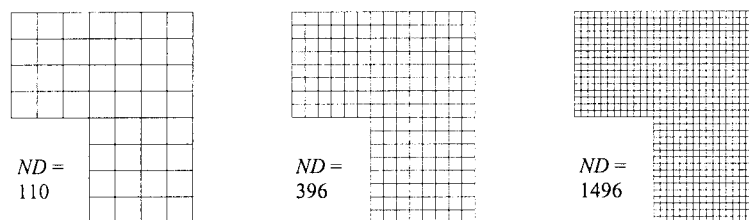Fig. 13 Mesh and results of a pressure vessel using AQV-element

Fig. 14 Uniform meshes for comparison

becomes better smoothed. It is obvious that the refined mesh using variable-node element makes it possible to catch the stress concentration near the corner using relatively small number of elements. For the purpose of comparison, the convergence using uniform meshes of Fig. 14 are also studied. The convergence curve which plots the relative percentage error vs. the number of nodes are presented in Fig. 15 which shows clear validation for the merits of the newly devised variable-node axisymmetric element.

5.2 Hanger socket

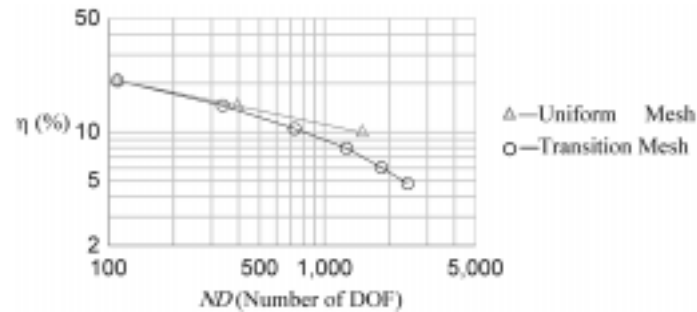A hanger socket is an important device for the anchorage of suspension bridges and other similar
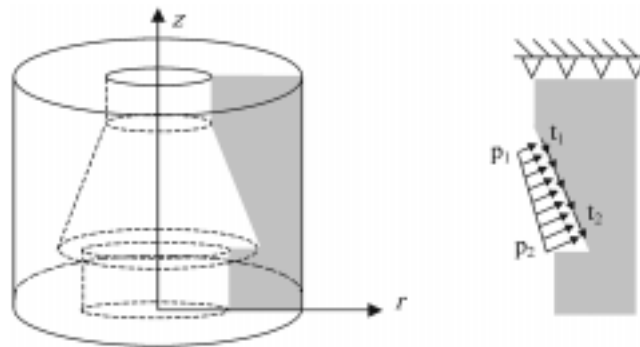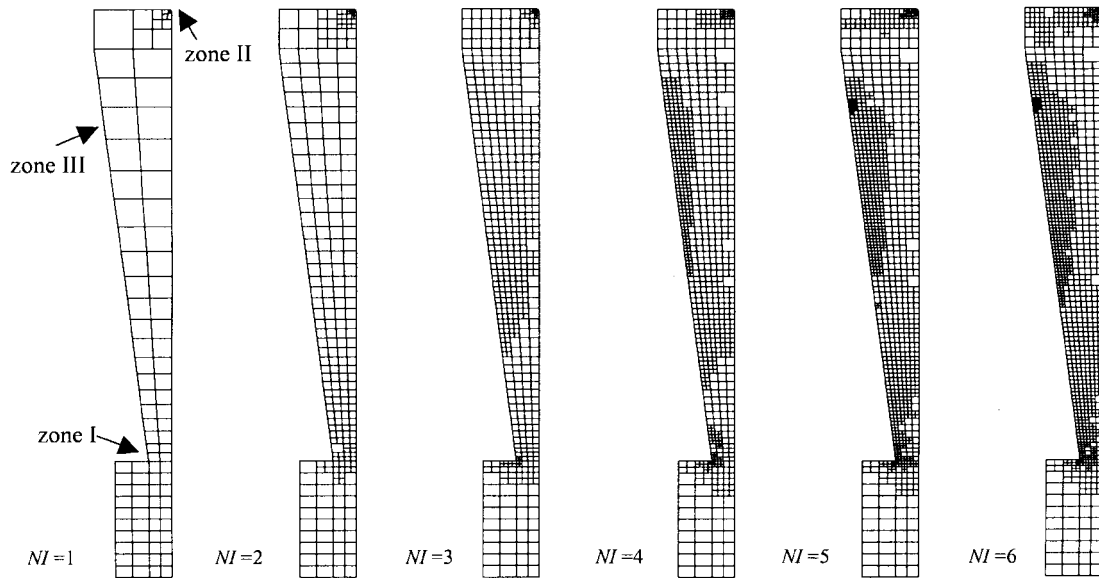
Fig. 15 Convergence curve

Fig. 16 An idealized hanger socket

structures. The loads of the girders are transmitted to the cable through hangers which are generally located by equal spacing. The ends of hangers are anchored by hanger sockets. A hanger socket consists of a steel cylinder with a conical cavity (Fig. 16). When the cable is subsequently subjected to tension, a wedge action will develop and a tri-axial state of stress in the cast material inside the cone will then efficiently promote the force transmission from the hanger to wires.

The simple sketch to show the idealized shape, boundary conditions and load conditions are given in Fig. 16. During the adaptive *h*-refinement process, the permissible relative error $\bar{\eta}$ of 5% is applied for each element. The refined meshes using AQV-element are shown in Fig. 17(a) and the deformed shapes are given in Fig. 17(b). In order to show the more detailed meshes and stress contours at three locations where the complicated transition zones are developed are enlarged in Figs. 18(a)-(c). The zone I is selected to catch the stress concentration due to the abrupt geometric change, the zone II shows the most severe stress concentration from boundary conditions, and the zone III from the large deformation due to the characteristic of loads. It shows that the variable-node element is very effectively used for efficient modeling.

6. Conclusions

In this study, the development and practical application of variable-node axisymmetric solid elements are presented. The formulation of variable-node axisymmetric element can be achieved by
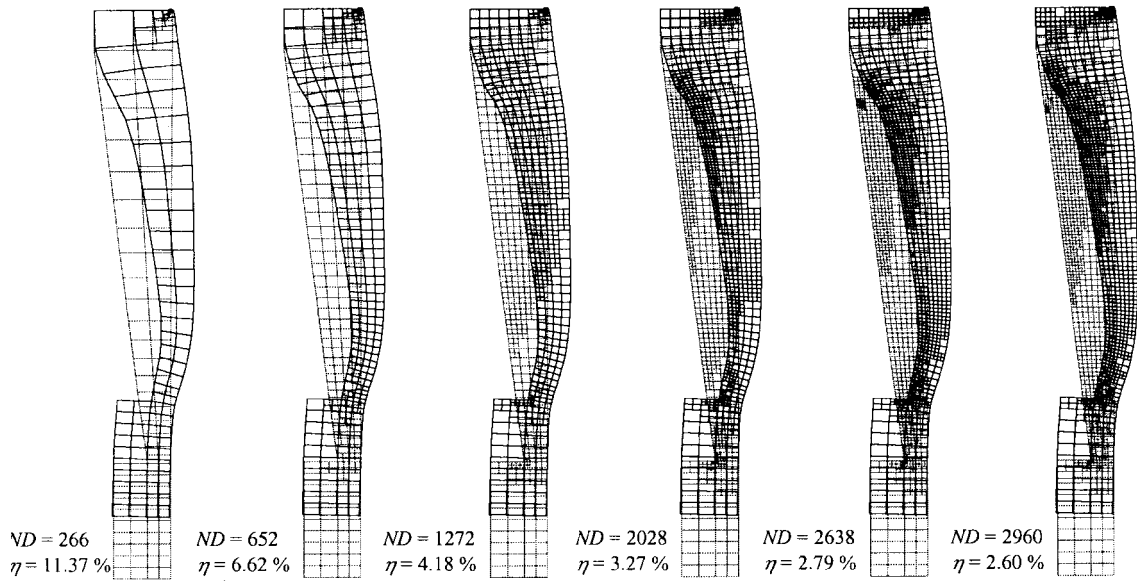
(a) Locally refine mesh

(b) Deformed shape (×1000)

Fig. 17 Mesh and results of a hanger socket

addition of midside nodes to the ordinary quadrilateral axisymmetric element and by creating new shape functions accordingly. A modified Gauss quadrature is needed to calculate the element matrices. These variable node-elements pass the basic element tests such as eigenvalue test and patch test which may indicate a good performance of the element. Some numerical test showed that the variable-node axisymmetric solid elements can be efficiently used in the adaptive mesh

(a) Meshes for zone I
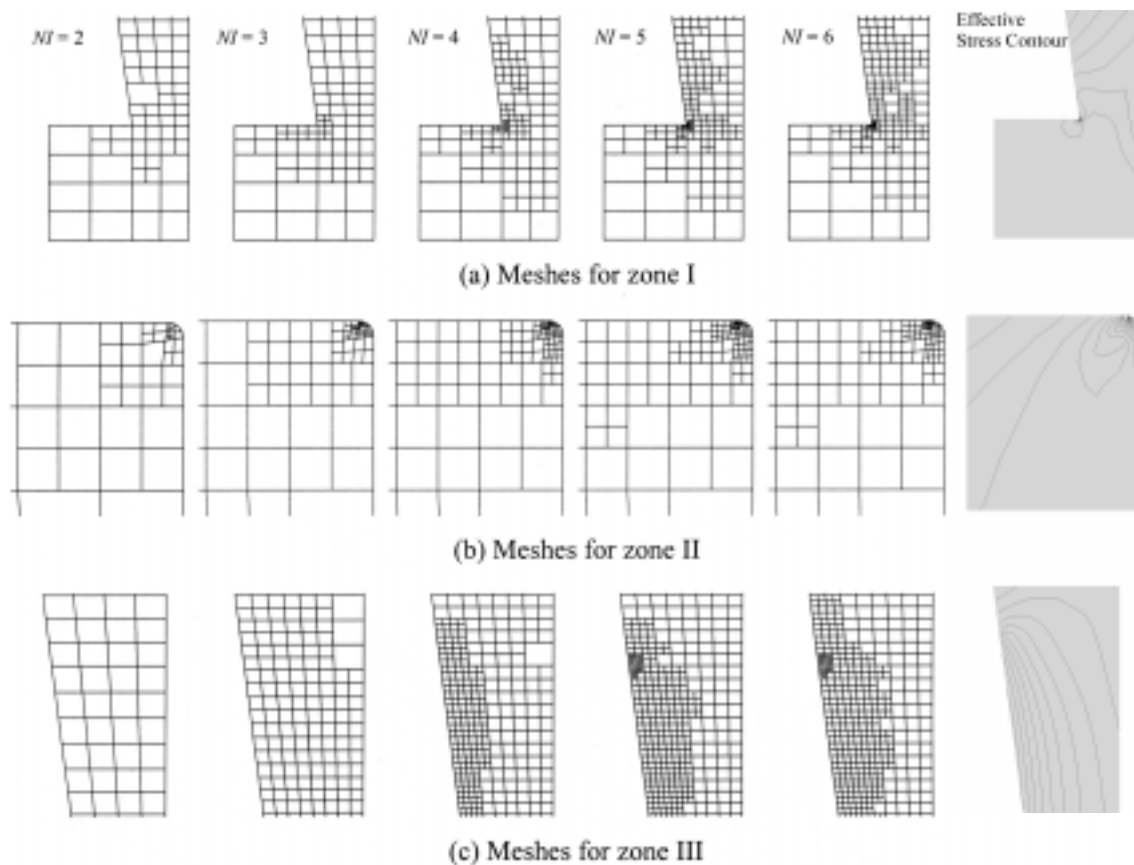

(b) Meshes for zone II

(c) Meshes for zone III

Fig. 18 Local mesh and effective stress contour

refinement for the axisymmetric structures without creating any hanging nodes which may cause some complications. The transition mesh generated by using variable node elements and the stress smoothing with modified superconvergent patch recovery produce a better convergence characteristics of solution. Several practical examples which have high stress concentrations due to the abrupt changes in geometry, boundary conditions, and load conditions were solved and the validity and applicability of the variable-node axisymmetric solid element to practical engineering problems were well demonstrated.

References

Bathe, K.J. (1982), *Finite Element Procedures in Engineering Analysis*, Prentice-Hall, New Jersey.

Hughes, T.J.R. (1987), *The Finite Element Method - Linear Static and Dynamic Finite Element Analysis*, Prentice-Hall, New Jersey.

Choi, C.K., and Park Y.M. (1989), "Nonconforming transition plate bending elements with variable mid-side nodes", *Comput. and Struct.*, *An Int. J.*, **32**(2), 295-304.

Choi, C.K., and Park, Y.M. (1992), "Transition plate bending elements for compatible mesh gradation", *J. Eng. Mech.* ASCE, **118**(3), 462-480.

Choi, C.K., and Kim, S.H. (1992), "Improvement of quadratic finite element for mindlin plate bending", *Int. J. Numer Meth. Eng.,* **34**(1), 197-208.

Choi, C.K., and Lee, N.H. (1993), "Three dimensional transition solid elements for adaptive mesh gradation"*, Struct. Eng. and Mech. An Int. J.,* **1**(1), 61-74.

Zhu, J.Z., Zienkiewicz, O.C., and Wu, J. (1991), "A new approach to the development of automatic quadrilateral mesh generation", *Int. J. Numer. Methods Eng.*, **32**, 849-866.

Yunus, S.M., Pawlak, T.P., and Wheeler, M.J. (1990), "Application of the Zienkiewicz-Zhu error estimator for plate and shell analysis", *Int. J. Numer. Meth. Eng.*, **29**, 1281-1298.

Evans, A., Marchant, M.J., Szmelterm J., and Weatherill, N.P. (1991), "Adaptivity for compressible flow computations using point embedding on 2-D structured multiblock meshes", *Int. J. Numer. Meth. Eng.*, **32**, 895-919.

Abel, J.F., and Shephard, M.S. (1979), "An algorithm for multipoint constrains in the finite element analysis", *Int. J. Numer. Methods Eng.*, **14**, 464-467.

Cook, R.D. (1981), *Concepts and Applications of Finite Element Analysis*, 2nd edn., John Wiley & Sons, New York.

Choi, C.K., and Lee, W.H. (1996), "Versatile variable-node flat-shell element"*, J. Eng. Mech.,* ASCE, **122**(5), 432-441.

Choi, C.K., and Lee, W.H. (1995), "Transition membrane elements with drilling freedom for local mesh refinements"*, Struct. Eng. and Mech. An Int. J.,* **3**(1), 75-89.

Gupta, A.K. (1978), "A finite element for transition from a fine to a coarse grid", *Int. J. Numer. Meth. Eng.*, **12**, 35-45.

Zienkiewicz, O.C., and Zhu, J.Z. (1987), "A simple error estimator and adaptive procedure for practical engineering analysis", *Int. J. Numer. Meth. Eng.*, **24**, 337-357.

Zienkiewicz, O.C., and Zhu, J.Z. (1989), "Error estimates and adaptive refinement for plate bending problems", *Int. J. Numer. Meth. Eng.*, **28**, 879-891.

Zienkiewicz, O.C., and Zhu, J.Z. (1992), "The superconvergent patch recovery and A posteriori error estimates. Part 1: The recovery technique", *Int. J. Numer. Meth. Eng.*, **33**, 1331-1364.

MacNeal, R.H. and Harder, R.L. (1985), "A proposed standard set of problems to test finite element accuracy", *Finite Elements Anal. Des.*, **1**, 1-20.

Wanji, Chen, and Cheung, Y.K. (1996), "The nonconforming element method and refined hybrid element method for axisymmetric solid", *Int. J. Numer. Meth. Eng.*, **39**, 2509-2529.